ANNUAL REVIEWS

Annual Review of Food Science and Technology

Advanced Techniques for Hyperspectral Imaging in the Food Industry: Principles and Recent Applications

Ji Ma,[1,2,3] Da-Wen Sun,[1,2,3,4] Hongbin Pu,[1,2,3] Jun-Hu Cheng,[1,2,3] and Qingyi Wei[1,2,3]

[1]School of Food Science and Engineering, South China University of Technology, Guangzhou 510641, China

[2]Academy of Contemporary Food Engineering, South China University of Technology, Guangzhou Higher Education Mega Center, Guangzhou 510006, China

[3]Engineering and Technological Research Centre of Guangdong Province on Intelligent Sensing and Process Control of Cold Chain Foods, Guangzhou Higher Education Mega Centre, Guangzhou 510006, China

[4]Food Refrigeration and Computerized Food Technology, University College Dublin, National University of Ireland, Agriculture and Food Science Centre, Belfield, Dublin 4, Ireland; email: dawen.sun@ucd.ie

Annu. Rev. Food Sci. Technol. 2019. 10:7.1–7.24

The *Annual Review of Food Science and Technology* is online at food.annualreviews.org

https://doi.org/10.1146/annurev-food-032818-121155

Keywords

hyperspectral imaging, imaging spectroscopy, food quality, food safety, image processing, spectrometry

Abstract

Hyperspectral imaging (HSI) is a technology integrating optical sensing technologies of imaging, spectroscopy, and chemometrics. The sensor of HSI can obtain both spatial and spectral information simultaneously. Therefore, the chemical and physical information of food products can be monitored in a rapid, nondestructive, and noncontact manner. There are numerous reports and papers and much research dealing with the applications of HSI in food in recent years. This review introduces the principle of HSI technology, summarizes its recent applications in food, and pinpoints future trends.

INTRODUCTION

Food quality and safety are not only related to the quality of life of human beings but may even affect societal stability, e.g., when food safety outbreaks occur. To ensure safety and high-quality food, advanced food detection techniques are needed. Human visual examination, which is subjective, laborious, and inconsistent, is still commonly used in the food industry. The general instrumental methods used for food detection are mainly analytical chemical methods, which are destructive, incapable of handling a large number of samples, and consume a lot of time. Therefore, a reliable, rapid, nondestructive, and noncontact food detection technology is what researchers want to develop.

The hyperspectral imaging (HSI) technique is one of the most popular advanced food detection techniques and has been investigated for more than twenty years. The basic principle of HSI is that spectral and spatial information are coalesced to present both chemical and physical information about food. There are numerous published articles demonstrating the potential of HSI in food detection, including in meat and meat products (Xie et al. 2016), aquatic products (J.-H. Cheng et al. 2017), fruits and vegetables (Yang et al. 2015), cereal (Sendin et al. 2018), and others (Vásquez et al. 2018). With the rapid development of computer science and other related disciplines as well as major improvements in optical sensors, there have been significant advances in the applications of HSI to food. Therefore, this article reviews the principle of HSI technology as well as its applications from 2014 to 2018.

PRINCIPLES OF HYPERSPECTRAL IMAGING

In the food industry, noncontact, nondestructive, and continuous optical techniques are extremely beneficial for online detection of food quality and safety. Optical characteristics, including chemical, physical, and morphological information, contain different optical formats such as spectroscopy and imaging.

Furthermore, spectroscopy is an essential method for determining the chemical and physical characteristics of food based on the overtone and combination vibrations in visible (VIS) and near-infrared (NIR) spectral regions (Cortés et al. 2017). However, imaging is powerful for determining the size, shape, textural features, and color characteristics of food and presents the physical information based on RGB and gray-level values (Vidal et al. 2013). It is also possible to enhance information representation by visualizing chemical distribution pixel by pixel. HSI has the ability to simultaneously acquire spectral and spatial information in one system and integrates the advantages of spectroscopy and imaging.

Hyperspectral Imaging

To better understand the principles of HSI, it is necessary to introduce some fundamental knowledge about the system and hyperspectral image acquisition strategies.

Hyperspectral cube. A hyperspectral image is a three-dimensional (3D) hyperspectral cube that includes two-dimensional spatial information (of x rows and y columns) and one-dimensional spectral information (of λ wavelengths). The hyperspectral cube is made of a series of discrete subimages at small interval wavelengths ranging from 400 to 2,500 nm and that contain VIS and NIR spectral regions. First, for each subimage (x, y) at one wavelength, there is spatial information of the spectral intensity (λ) at that wavelength. Second, for each pixel (x, y), the full wavelength

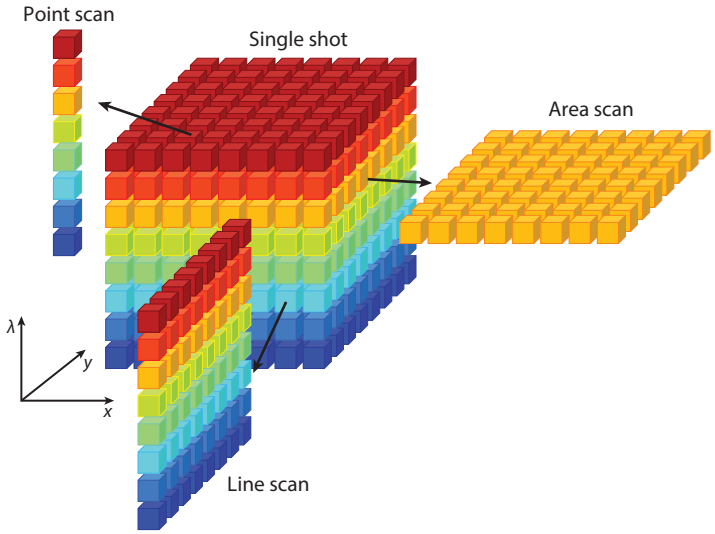

Figure 1

Four hyperspectral image acquisition strategies: point scanning, line scanning, area scanning, and single shot.

spectrum is obtained. The above two perspectives are the most common strategies for studying hyperspectral cubes (Wu & Sun 2013).

Acquisition strategies of hyperspectral image. A 3D hyperspectral image can be obtained through four HSI acquisition strategies, which are the point-scanning, line-scanning, area-scanning, and single-shot methods, as shown in **Figure 1**. The point-scanning, or whiskbroom, method records the spectral information of the image pixel by pixel by moving the detector or samples along the two spatial dimensions (x and y). The point-scanning method is appropriate for obtaining high spectral resolution and a stable hyperspectral image, but the scanning speed is low. The storage format of the point-scanning method is band-interleaved-by-pixel (BIP) format.

The line-scanning, or pushbroom, method is the most common HIS strategy. A whole line, including spectral information, is scanned one by one continuously by linearly moving samples or the detector. The moving direction (x) should be perpendicular to the scanning line, and the resulting image is stored in the format of band-interleaved-by-line (BIL) format. Most of the HSI applications mentioned below follow the line-scanning mode.

Another approach is the area-scanning method, which is also called the wavelength-scanning method. Using the area-scanning method, a two-dimensional (x and y) gray-level image at one wavelength can be acquired, and an area-scanning hyperspectral image can be acquired by scanning gray-level images over the whole wavelength range. The storage format is the band-sequential (BSQ) format. The scanning speed of this mode is fast when using previously selected wavelengths.

The single-shot method obtains all spectral and spatial information of a hyperspectral image simultaneously with one exposure. The scanning speed is the fastest, and a hyperspectral video can be recorded. However, because of the limitations of the single-shot device, it is difficult to make the spatial and spectral resolutions meet the demands of the food industry (Nicolaï et al. 2007).

Hardware of Hyperspectral Imaging

The hardware of an HSI system plays a significant role in the acquisition of hyperspectral image data and reliable, efficient, and high-quality information. A typical HSI system commonly needs light sources, wavelength dispersion devices, and area detectors.

Light sources. Various options for HSI light sources can be selected under different operating conditions. Halogen lamps are broadband illumination sources covering the VIS–NIR spectral regions. Halogen lamps working with low voltage are considered an all-purpose illumination source because the spectrum of the halogen lamps light is smoothing and continuous without sharp peaks. However, the shortcomings of halogen lamps include high heat effects, short lifetime, and spectral peak shift due to temperature and voltage changes (Pu et al. 2015). Light-emitting diodes (LEDs), which are made from semiconductor material, have been introduced as illumination sources for HSI systems because of their small size, fast response, long lifetime, and low cost, heat generation, and energy consumption. LEDs have the ability to produce various types of light, including narrowband light at different single wavelengths in the ultraviolet, visible, and infrared regions and broadband light at different intensities as well as different arrangements of spot, line, and ring lights. The disadvantages of LEDs include low heat dissipation efficiency and high environmental temperature, which can affect the lifetime of LEDs because of earlier luminous attenuation. There are also differences in, e.g., color, brightness, and bias voltage among each single LED in an LED array (Park et al. 2011).

Wavelength dispersion devices. Dispersion devices are an essential component of an HSI system for dispersing broadband light into different wavelengths. In principle, there are three kinds of wavelength dispersion devices: monochromator, optical bandpass filter, and single-shot imager. Monochromators are basic dispersion devices that divide polychromatic light into the integral spectrum. The most frequently used monochromators in line-scanning HSI systems are prisms and diffraction grating. Prisms can refract light of different wavelengths into different angles to disperse a white beam into different wavelength bands. A diffraction grating consists of a periodic structure that modulates the amplitude or phase (or both) of the incident light cyclically and spatially. Such a grating can be transmitting or reflective. Another monochromator, called the prism-grating-prism (PGP), is able to avoid surface reflection and block unwanted wavelengths and is made up of a short-pass filter prism, transmission grating, and long-pass filter prism. Furthermore, optical bandpass filters, including fixed and tunable filters, are commonly used for area-scanning HSI systems. The fixed bandpass filters, such as filter wheels, carry a set of particular interference filters. The filter wheels are especially suitable for the multispectral systems, but they have their disadvantages, e.g., small spectral range, low resolution, fast wavelength shift, and image distortion during the movement of the filter. The tunable filters, such as the liquid crystal tunable filter (LCTF) and acousto-optic tunable filter (AOTF), can be electronically controlled for high-wavelength tuning speed and image quality. LCTFs are made of a series of tunable retardation liquid crystal plates between two parallel polarizers working from the VIS to NIR region. AOTFs consist of a birefringent crystal, tunable radio frequency source, and piezoelectric crystal transducer and absorber, covering the wavelength range from UV to IR. Compared with AOTFs, LCTFs have lower wavelength switch speed but higher image quality. Single-shot imagers, which are wavelength dispersion devices, are used to implement the single-shot HSI system. In the single-shot imager, each pixel cell consists of a 2D grating array to obtain both spectral and spatial information at the same time (Wu & Sun 2013).

Area detectors. The area detector is the photosensitive element in HSI systems. Area detectors have the ability to quantify the intensity of light by transforming light signals into analog current signals. Charge-coupled device (CCD) and complementary metal oxide semiconductor (CMOS) cameras are two commonly used area detectors in HSI systems, and both are made of photodiodes. The differences between these two detectors are the digital signal transmission methods. In the CCD sensor, the charge of each pixel is sequentially transmitted to the next pixel, output from the bottom-most portion, and then amplified by an amplifier at the sensor edge. In the CMOS sensor, each pixel is adjacent to an amplifier and A/D (analog to digital) converter circuit. The differences between CCD and CMOS are that CCD performed better than CMOS in sensitivity, resolution, power, and cost, whereas CMOS performed better in noise.

Basic Hyperspectral Imaging Processing Steps

HSI data analysis relies on mathematical calculation because the hyperspectral image is large and suffers from collinearity problems. Chemometric algorithms are applied for essential data mining. The common steps for HSI data processing and analysis are presented in **Figure 2**.

Treatment of sample and measurements of sample components. Samples for HSI do not require particular preparation. However, as the NIR region is sensitive to water, it is necessary to control the surface moisture of the samples. Additionally, to obtain a series of accurate data, analytical measurements of components using traditional methods should be performed with care and caution because the experimental measurement of component concentrations is regarded as an important step in establishing the final HSI prediction model.

Hyperspectral image acquisition and processing. As discussed above, there are four image acquisition strategies (Nicolaï et al. 2007), and three common image-sensing modes, i.e., reflectance, transmittance, and interactance, for HSI are available (see **Figure 3**). The differences among the three modes are in the position and arrangement of the light sources, optical detectors, and samples. In reflectance mode, the light source and the optical detector are on the same side of the sample, and the location of the light source and the optical detector should be tuned to avoid specular reflection. In this mode, the external quality attributes of size, shape, color, surface texture, and external defects can be easily detected. In transmittance mode, the light source and optical detector are on both sides of the sample. Transmittance mode plays a significant role in the internal quality evaluation of, e.g., internal component concentration and defects; however, the signal is influenced by the thickness of the sample and is often weak. In interactance mode, the light sources and the optical detector are on the same side of the sample, but the field of vision of the optical detector is not illuminated. The light is captured by the optical detector when it passes through the sample and reaches the surface. Therefore, in this mode, both external and internal information can be obtained, and the effects of specular reflection and sample thickness can be avoided.

After capturing a raw hyperspectral image, that image is calibrated in terms of wavelength, spatial aspects, curvature, and reflectance. The calibrated image is then segmented by a thresholding, morphological processing, or edge-based segmentation algorithm to obtain a region of interest (ROI).

Image processing. Several image-processing strategies can be used to obtain useful information from the image. First, a series of images at typical wavelengths can be used to detect the surface defects or properties because these defects or properties appear only on certain bands. Second,

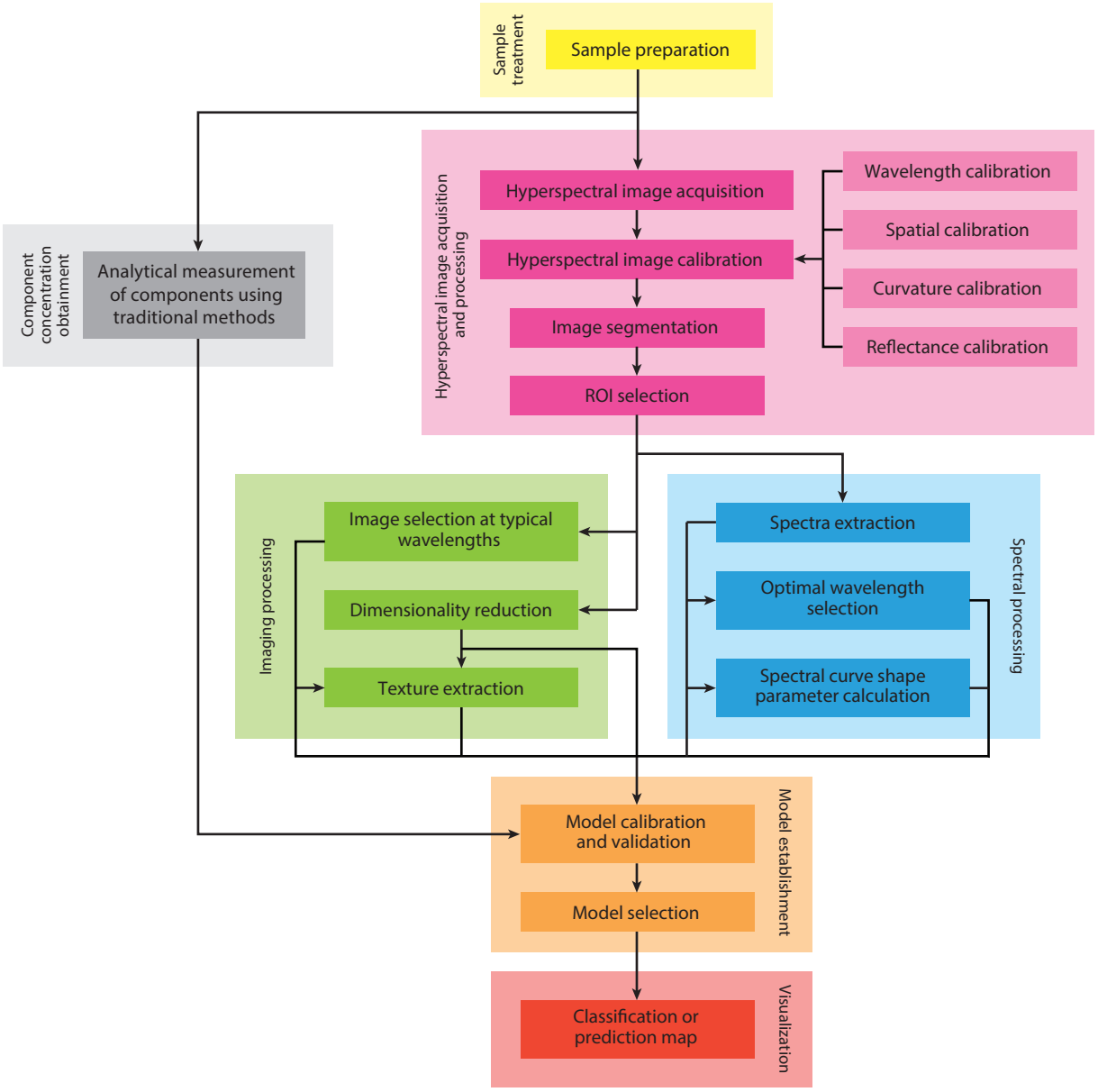

Figure 2

Common steps for hyperspectral imaging operation processing and data analyzing include sample treatment, component concentration obtainment, hyperspectral image acquisition and processing, imaging and spectral processing, model establishment, and visualization. Abbreviation: ROI, region of interest.

principal component analysis (PCA) and the independent component correlation algorithm (ICA) are applied to calculate the PCA and ICA images, respectively. A few principal component (PC) images or independent component (IC) images are selected to identify the surface defects. Lastly, textural features can be quantified by texture algorithms in images of typical wavelengths, PC images, or IC images.

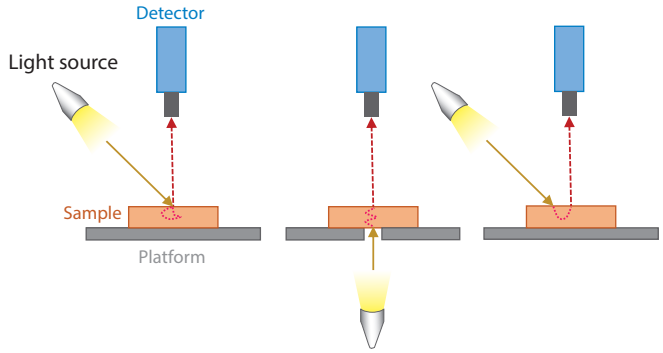

Figure 3

Image-sensing modes of hyperspectral imaging: reflectance, transmittance, and interactance.

Before imaging analysis and depending on the image quality, an optional program can be applied to enhance the image by using suitable methods such as Fourier transform (FT) and wavelet transform (WT). It should be noted that whether selecting images at typical wavelengths or using computed PC or IC images, the core of the image processing is dimensionality reduction because a hyperspectral image is too large to obtain useful information directly.

Spectral processing. In the process of capturing hyperspectral images, some negative effects, e.g., random noise, length variation of the light path, and useless light scattering, are unavoidable. Therefore, a number of spectral preprocessing algorithms are applied to solve this problem. In addition, hyperspectral images have high resolution in the spectral dimension and the interval between the bands is very small; thus, the collected wavelengths can be regarded as continuous. Continuous wavelengths can lead to collinearity problems, indicating that the independent variables are highly correlated, resulting in the weakening of the accuracy of the model. Hence, selecting optimal wavelengths can not only remove the low signal-to-noise ratio (SNR) bands but also extract the most representative wavelengths as well as reduce the spectral dimension.

Another strategy for spectral dimension reduction is to calculate some parameters of the spectral curve shape. The overall trend of the spectral curve can be considered globally. In short, the purposes of spectral processing and image processing are similar, except that similar treatments are performed on different dimensions of hyperspectral images.

Model establishment. The desired information about the sample cannot be obtained directly from a 3D hypercube, and chemometric models can correlate the hyperspectral image with the desired properties. Because of the huge amounts of HSI data, the mean spectrum of all pixels within the ROI is usually used to build a model. Generally, there are two types of models in HSI data analysis: classification models and regression models. The classification model is used to divide targets into discrete finite known or unknown groups to, for example, classify samples obtained under different processing conditions or grade samples into different classes. However, the regression model establishes a relationship between input data and target properties in a continuous range, such as component concentration prediction. The regression model can be used to classify samples by setting one or several thresholds to, for example, grade samples based on the value of one or several components.

Visualization. Visualization of chemical imaging is a unique feature of HSI. Compared with image and spectroscopy, chemical imaging is the most characteristic expression of HSI images. With the imaging method, the appearance information of a sample can be known, but its chemical information cannot be obtained. For the spectroscopic method, only the average chemical information of the whole sample can be attained, but its distribution cannot be found. However, using HSI, the value of quality attributes of each pixel can be calculated by the model established, and the predictive value can then be presented using a false color image. Therefore, the chemical contents of a sample and their distributions can be visually observed by the color change in the false color image.

Algorithms

Algorithms are the most important support methods for HSI, from the capturing of images to the presentation of final results. Among different processing steps, HSI algorithms can be divided into the following main categories: image calibration algorithms, spectral processing algorithms, image-processing algorithms, and chemometric model algorithms. An overview of these algorithms is shown in **Table 1**.

Image calibration algorithms. After the acquisition of a raw hyperspectral image, it is necessary to carry out reflectance calibration to calibrate the raw intensity image into the reflectance or absorbance image with black and white reference images and remove the effect of the dark current of the camera. The dark image is captured by switching off the light sources and covering the camera lens cap, and the white image is obtained under the condition of raw image acquisition by using a white surface board, which is usually made of Teflon, with a uniform, stable, and high reflectance standard. The calibration algorithm is achieved using the following equation:

$$R = \frac{I_S - I_D}{I_W - I_D} \times 100\%, \qquad 1.$$

where R is the calibrated hyperspectral image, I_S the raw hyperspectral image, I_W is the white reference image, and I_D is the dark reference image.

Spectral processing algorithms. Spectral processing involves spectral preprocessing and spectral features extraction. Spectral preprocessing algorithms are used to improve the spectral data. The widely used algorithms include smoothing, detrending, derivatives, multiplicative scatter correction (MSC) (Isaksson & Næs 1988), and standard normal variate (SNV) (Barnes et al. 1989) as well as others. Several smoothing methods, including Savitzky–Golay, moving average, and median filter, are used to reduce the spectral noise without changing the amounts of spectral data. Detrending is accomplished by removing the baseline drift of the diffuse reflectance spectrum. Derivatives (normally first and second derivatives) are applied to correct baseline effects, remove background interference, and improve spectral resolution, which can be achieved by the Savitzky–Golay and Norris methods. MSC and SNV have similar functions in that they reduce the length variation of the light path and useless light scattering.

Optimal wavelength selection algorithms are used to decompose the dimension, produce the smallest possible errors, and enhance the useful information of the spectra. The most common way is to use regression coefficients of the optimal model that belongs to partial least squares regression (PLSR) or principal component regression (PCR) to extract the optimal wavelengths with large absolute values in peaks and troughs (Liu et al. 2014d). Another simple method, defined as an analysis of spectral differences, is to calculate the differences among various samples

Table 1 Overview of algorithms used in hyperspectral imaging data analysis

Hyperspectral imaging processing steps	Algorithms	References of applications in recent years
Spectral preprocessing algorithms	Savitzky–Golay (SG) smoothing	Ma et al. 2017a
	Moving average smoothing	
	Median filter	Mohammadi-Moghaddam et al. 2018
	Detrending	Caporaso et al. 2018a
	First derivatives	Liu et al. 2018b
	Second derivatives	Zhao et al. 2017
	Multiplicative scatter correction (MSC)	Xie et al. 2015
	Standard normal variate (SNV)	Su & Sun 2017
	Orthogonal signal correction (OSC)	Rady et al. 2015
	Wavelet transform	Yang et al. 2018
Optimal wavelengths selection algorithms	Regression coefficients (RC) of partial least squares regression (PLSR)	Liu et al. 2014b
	Successive projections algorithm (SPA)	Li & Chen 2017
	Uninformative variable elimination (UVE)	Qu et al. 2015
	Genetic algorithms (GAs)	Yang et al. 2015
	Spectral absorption index (SAI)	Ma et al. 2016
Image-processing algorithms	Principal component analysis (PCA)	Zhang et al. 2018
	Histogram statistics (HS)	Pu et al. 2015
	Gray-level co-occurrence matrix (GLCM)	Qu et al. 2015
	Gray-level gradient co-occurrence matrix analysis (GLGCM)	Ma et al. 2015
	Wavelet transform	Pu et al. 2015
Classification model algorithms	PCA	Wu et al. 2016a
	K-means	
	Hierarchical clustering	
	Linear discrimination analysis (LDA)	Li et al. 2016a
	Partial least square discriminant analysis (PLS-DA)	Ma et al. 2015
	Support vector machines (SVM)	zhang et al. 2016
	k-nearest neighbor (kNN)	Rady et al. 2015
	Soft independent modeling of class analogy (SIMCA)	Qu et al. 2015
	Random forest	Qu et al. 2015
Regression model algorithms	Multiple linear regression (MLR)	Liu et al. 2014c
	Principal component regression (PCR)	Mahesh et al. 2015
	PLSR	Mahesh et al. 2015
	Artificial neural networks (ANN)	Yang et al. 2015
	Support vector regression (SMR)	Chen et al. 2015
	Least squares support vector machines (LS-SVM)	Yang et al. 2017b

to select the important wavelengths with large differences between samples of different varieties for the discrimination of the significant and insignificant wavelengths. Stepwise regression analyzes the significance of wavelengths to save the optimal wavelengths by adding wavelengths one by one and testing the model to remove the insignificant wavelengths (Cluff et al. 2008). The successive projections algorithm (SPA) uses projection analysis to compare the projection

of each wavelength at other wavelengths and obtains the final optimal wavelengths with minimum redundancy information and minimum collinearity using a calibration model (Araújo et al. 2001). Uninformative variable elimination is based on the regression coefficients of PLSR, which eliminate useless variables and keep useful variables (optimal wavelengths) (Centner et al. 1996). Furthermore, other methods, including simulated annealing (Chen & Lei 2009), genetic algorithms (Leardi et al. 1992), mutual information (Rossi et al. 2006), and interval base algorithms (Norgaard et al. 2000), are also powerful algorithms for optimal wavelengths selection. Parameters of the spectral-curve-shape-calculating algorithms are useful methods to decompose the spectral dimension and extract useful information. Finally, the spectral absorption index is a comprehensive index used for describing spectral absorption features extracted from spectral curves by analyzing the relationships of value and the position of peaks and troughs (Ma et al. 2016).

Image-processing algorithms. Image compression and characteristics extraction are common analysis methods for hyperspectral image processing. PCA transforms variables into a new coordinate system through a linear transformation so that the largest variance of any data projection is on the first coordinate, the second largest variance is on the second coordinate, and so on, leading to the obtaining of the same number of principal components compared with raw data. PCA is used to calculate PC images in hyperspectral image processing and can also be used to compress images. The first few PC images (typically fewer than three to five images) usually contain as much as 98% of the information of the whole hypercube (Wang et al. 2015). ICA separates the data into a linear combination of statistically independent non-Gaussian source signals through a linear transformation to separate independent signals as much as possible.

Image texture-based processing algorithms are used to quantify image information. The statistical matrix of the gray-level histogram is the simplest description method of the texture. It has no information about the position of the texture in space and cannot describe the spatial relationship of the texture image. The parameters extracted from a gray-level histogram include mean, variance, and entropy. The gray-level co-occurrence matrix (GLCM) is the most widely used statistical texture analysis method (Qu et al. 2015). It considers the spatial position of pixels in the image and uses the correlation between pixels to obtain different textural feature parameters to represent these relationships. Gray-level-gradient co-occurrence matrix (GLGCM) analysis focuses on the two most basic elements of an image, namely the gray level and gradient (or edge) of the image points (Ma et al. 2015). The gray level of each pixel is the basis for forming an image, and the gradient is the element that constitutes the outline of the image edge. Therefore, compared with GLCM, GLGCM adds the gradient element to enhance the texture quantification.

Chemometrics model algorithms. Classification (also called pattern recognition), which includes unsupervised and supervised classification, is the qualitative analyzing method. Multivariate classification can be unsupervised or supervised. Typical unsupervised classification methods in HSI analysis contain PCA, k-means clustering, and hierarchical clustering. Unsupervised classification methods are established without a priori knowledge about the calculated information by analyzing the natural characteristics of the data. PCA is the most commonly used algorithm in pattern recognition, and the first several PCs can be applied to achieve pattern recognition (Wold et al. 1987). k-Means clustering divides samples into set k clusters based on the minimum distance to the cluster centroid. Hierarchical clustering adopts a noniterative hierarchical clustering strategy. It considers each sample as a cluster, then calculates the distance between clusters and classifies two or more similar clusters into one until all samples are classified as one, and a hierarchy of clusters is then built by withdrawing a dendrogram.

Typical supervised classification algorithms include linear discrimination analysis (LDA), partial least square discriminant analysis (PLS-DA), support vector machines (SVMs), and k-nearest neighbor (kNN). Supervised classification methods are applied with known calculated information by measured characteristics. LDA analyzes the best linear projection based on the smallest intraclass and largest extraclass variance of the independent variables to separate the samples into different categories (Izenman 2008). PLS-DA is based on the PLSR method and uses a dummy variable to perform the optimal classification of PLSR-dependent variables (Ma et al. 2015). SVM classifies samples by finding the best compromise between the complexity of the model (the learning accuracy of particular training samples) and the ability to learn (the ability to identify any sample without error) based on limited sample information (Vapnik 2013). In the kNN algorithm, if most of the k-nearest samples in the feature space belong to a certain category, the sample also belongs to that category.

Regression is a quantitative analyzing method that includes both linear and nonlinear regression. Linear regression algorithms mainly contain multiple linear regression (MLR), PCR, and PLSR. MLR builds a simple and easily understood linear relationship between spectra and the measured properties of the samples. It is worth noting that MLR works only when the number of samples is less than that of variables, which is easily influenced by the collinearity among variables. PCR combines PCA and MLR. PCR builds a model based on MLR with the variables of independent PCs under PCA. The disadvantage of PCR is that PCA is an unsupervised method that does not consider the reference values of dependent variables; thus, the calculated PCs may not contribute to the dependent variables. PLSR decomposes both independent and dependent variables at the same time to evaluate the linear relationship between them (Wood et al. 2004). Raw data are linearly transformed into new orthogonal and uncorrelated variables called latent variables (LVs). The LVs are sorted by their contribution and the first several sorted LVs are most related to the dependent variables. Therefore, choosing the optimal number of LVs that have the best prediction accuracy is the way to achieve regression.

However, the spectra of samples and the tested properties may follow a nonlinear relationship. Artificial neural networks (ANNs), SVMs, and least squares support vector machines (LS-SVMs) are the most used nonlinear regression algorithms. ANN is an algorithm that simulates the structure and function of a neural network of animals through artificial learning so as to implement an algorithm for quick and accurate information processing. A neural network is an operational model consisting of a large number of nodes (or neurons) connecting to each other, including input, hidden, and output nodes. Each neuron represents a specific output function, called an activation function. The connection between every two neurons represents a weighted value for the signal, called the weight, which is equivalent to the memory of the ANN. The output of the network depends on the weight value, the incentive function, and how the network is connected. Thus, the spectra are introduced to the input layer, and the results of the predicted values are obtained from the output layer. LS-SVM is based on SVM by optimizing the inequality constraint function into equality. Lagrange multiplier is used to calculate the partial differentiation of each feature to obtain the optimal solution. ANN and SVM can be utilized in both classification and regression situations.

RECENT APPLICATIONS OF HYPERSPECTRAL IMAGING

The HSI technique has been investigated as a beneficial analytical method for fast, nondestructive, and noncontact analysis for assessment of the quality and safety of meat and meat products, fruits and vegetables, aquatic products, cereals, and others. Several books and reviews summarizing the

applications of HSI from different perspectives are also available; thus, only new applications since 2014 are discussed in this review.

Chemical and Physical Analyses

The physical and chemical characteristics of foods are closely related to the quality and safety of foods, and thus determining these physical and chemical properties, which include moisture contents, protein-related substances, fat-related substances, carbohydrate content, textural features, and other properties, is important for food evaluation.

Moisture contents. Water is an indispensable solvent component for all living organisms, and it is also a major component of foods. The content, distribution, and state of moisture in food have a great influence on food structure, appearance, texture, flavor, and freshness and have a significant impact on the value of food products. Therefore, monitoring moisture contents and their change in food by HSI is significant.

It is feasible to evaluate the moisture content of meat and meat products. The moisture content of pork meat under different processes was investigated by HSI using optimal wavelengths (Liu et al. 2014c), parameters of the spectral curve shape (Ma et al. 2016), and textural features (Ma et al. 2017b), and simple models were established with the coefficients of determination of prediction (R^2_p) of 0.969, 0.952, and 0.949, respectively. Iberian dry-cured ham was studied to map the moisture content distribution (Garrido-Novell et al. 2015). The Monte Carlo variable selection (MCVS) method was applied to HSI data analysis to estimate the moisture content of ground beef with an R^2_p of 0.99 (Zhao et al. 2017). The ANN model was carried out to fuse spectral and textural information to evaluate the moisture content of cooked beef with an R^2_p of 0.977 (Yang et al. 2017a). Additionally, the moisture contents of both a river fish (*Ctenopharyngodon idella*) (Qu et al. 2017) and sea fish (salmon) (Zhu et al. 2014) were successfully detected by HSI technique.

HSI has also been applied to fruit and vegetables with high moisture contents. Lychee is a tropical fruit with high moisture and saccharide contents and a short shelf-life. Radial basis function–support vector regression (RBF-SVR) algorithms were first applied to establish a predictive model for evaluating the moisture content of lychee with peel (Yang et al. 2015). Dried-sliced fruits such as apple (Crichton et al. 2017) and mango were analyzed to map the moisture distribution. Different shapes of mango (Pu & Sun 2015, 2017) were used to study the shape effects on moisture migration (Pu & Sun 2016). It is also feasible to investigate the moisture contents of other agricultural products such as vegetable bean (Huang et al. 2014) and purple-fleshed sweet potato (Sun et al. 2017b) with a correlation coefficient of prediction (R_p) of 0.971 and an R^2_p of 0.984. Additionally, HSI was widely applied to evaluate moisture contents in other foods, e.g., coffee beans (Amjad et al. 2018, Caporaso et al. 2018b), peanut kernels (Jin et al. 2015), pistachio kernels (Mohammadi-Moghaddam et al. 2018), and tea (Deng et al. 2015).

Protein-related substances. Proteins have a major impact on the texture, flavor, and processing traits of foods, mainly because proteins have different functional properties. A classification model was established in the region of 900–1,700 nm to discriminate proteins among pork, poultry, and fish. The classification model based on single classification tree presented better performance in a validation set with a correct classification rate (CCR) of 92% than using PLS-DA with a CCR of 90% (Garrido-Novell et al. 2018). Protein contents of different processed pork meat were evaluated by using a single-shot HSI sensor with a determination coefficient of cross-validation set (R^2_{CV}) of 0.8318 (Ma et al. 2019). Myofibrillar proteins are an important component of

muscle protein. The structure deformation degree of pork myofibrillar under frozen processing was characterized by evaluating surface hydrophobicity (S_0ANS) and Ca^{2+}-ATPase activity, and acceptable predictive models based on SPA-PLSR combined with spectral angle mapping were built to predict S_0ANS and Ca^{2+}-ATPase activity with R^2_p of 0.986 and 0.879, respectively (Cheng et al. 2018a). Oxidative damage of pork myofibrils was also monitored by evaluating the protein carbonyl content using a PLSR model with an R^2_p of 0.856 (Cheng et al. 2018b). Furthermore, protein contents of more than 3,250 single kernels of wheat were analyzed and the best PLSR model was based on SNV + first derivative with R^2_p of 0.82 (Caporaso et al. 2018a). Additionally, edible bird's nest is a precious functional and high-value-added food in Southeast Asia. The protein content of edible bird's nest was investigated by establishing a PLSR model with an R^2_p of 0.82 (Shi et al. 2017).

Amino acids are the basis of protein. The amino acid content of potato was predicted by a tenfold cross-validation PLSR model with an R^2_p higher than 0.90 (Kjær et al. 2016). Collagen is a significant component of connective tissues of beef meat. The feature amino acid of collagen called hydroxyproline was evaluated to quantify collagen contents by means of the PLSR model (Xiong et al. 2015c). Furthermore, total volatile basic nitrogen (TVB-N) refers to the fact that during storage the decomposition of animal foods is due to enzymes and bacterial substrates that break down proteins to produce basic nitrogenous substances such as ammonia and amines, which are the main freshness indicator of meat. There are many articles published about TVB-N detection via application of HSI to identify the freshness of fish (Cheng et al. 2014, J.-H. Cheng et al. 2017), pork (W. Cheng et al. 2017, Guo et al. 2018, Lee et al. 2018, Li et al. 2015), chicken (Khulal et al. 2016, 2017), duck (Qiao et al. 2017), prawn (Dai et al. 2015), and cured pork (Yang et al. 2017b).

Fat-related substances. Fat has an important function for storing energy and is biologically active. The detection applications of fat-related substances are mainly focused on meat and meat products. Fat content is an important criterion in beef grading. A PLSR model was established to evaluate the fat content in ground beef with an R^2_p of 0.99 (Zhao et al. 2017). Marbling is another vital feature relating to the quality of beef, which is defined by the visible fat distribution on the surface. Marbling of beef was researched by means of chemical analysis based on fat-content prediction and its distribution mapping and physical analysis via the classification of pixels on a high-contrast wavelength between fat and meat (Lohumi et al. 2016, Velásquez et al. 2017). Ma et al. (2018) reported a novel spectral preprocessing method [correlation optimized warping (COW)] to enhance the HSI data for protein contents predicting of cooked pork meat with an R^2_P of 0.9635. Additionally, intramuscular fatty acid contents of lamb were determined by using tenfold cross-validation with Monte Carlo algorithm partition for a calibration set and a cross-validation set (Craigie et al. 2017). Salmon has always been considered a highly nutritious fish. Detecting the fat (Zhu et al. 2014) of salmon and the fatty acid (Tao et al. 2017) contents of salmon and grass carp (Cheng et al. 2019) is feasible using HSI and reliable. Furthermore, the lipid contents of coffee beans (Caporaso et al. 2018b) and peanuts (Yu et al. 2016) were also evaluated by HSI.

Fat oxidation is inevitable for muscle food during storage, and 2-thiobarbituric acid (TBA) is a significant oxidative parameter that shows the degree of fat oxidation. Normally, TBA was evaluated by determining its reactive product. Muscle foods such as pork (Wu et al. 2016b), chicken (Xiong et al. 2015b), fish (Cheng et al. 2015), and processed sausages (Siripatrawan 2018) were investigated by evaluating their TBA content to identify the freshness level during storage.

Carbohydrate contents. Applications for detecting carbohydrates are mainly focused on fruits and vegetables. The term soluble solids normally refers to soluble saccharides, which are the main ingredient in carbohydrates in foods. Apple is one of the most popular fruits all over the world

because of its extensive planting, delicious taste, and rich nutrition. The soluble solid content (SSC) of apple was determined by HSI (using PLSR models) at wavelengths ranging from 400 nm to 2,500 nm, with performances of $R_p > 0.9327$ (Fan et al. 2016a,b; Ma et al. 2017d). Furthermore, the SSC of pear was investigated (Fan et al. 2015; Li et al. 2016a,c), and the best predictive model was based on SPA-PLSR and ranged from 400 nm to 1,000 nm with an R_p of 0.9924 (Li et al. 2016a). The carbohydrate content of kiwifruit was assessed by predicting the SSC (Guo et al. 2016) and sugar accumulation contents (Hu et al. 2017). The full spectra, ranging from 400 to 1,000 nm, were used to predict the SSC of kiwifruit via the LS-SVM method with an $R_p = 0.971$ (Guo et al. 2016). The optimal wavelengths were selected to evaluate sugar, including glucose, fructose, and sucrose, accumulation in kiwifruit, with results of R^2_p of 0.934, 0.867, and 0.705, respectively (Hu et al. 2017). Additionally, applications of SSC predictions in peach (Li & Chen 2017), lychee (Pu et al. 2016), banana (Pu et al. 2018), citrus (Teerachaichayut & Ho 2017), potato (Rady et al. 2015) and tomato (Rahman et al. 2017) were widely carried out using HSI. Finally, the insoluble and soluble dietary fiber contents of celery (Yan et al. 2017) predicted using the PLSR model were R_ps of 0.964 and 0.976, respectively.

Textural features. The textural features of food play a crucial role in food quality evaluation. There are numerous methods to present the textural feature of foods, including the three-point bending test; single-edge notched bend (SENB) test; compression and puncture tests, such as the texture profile analysis (TPA) and Magness–Taylor (M-T) puncture tests; Warner–Bratzler shear force (WBSF) and slice shear force (SSF) tests, and other destructive methods. Typically, TPA, WBSF, and SSF are the most popular textural features that can be predicted nondestructively by an HSI system. The TPA test simulates how samples behave when chewed by being compressed twice using a texture analyzer, which includes common parameters of hardness, springiness, cohesiveness, gumminess, chewiness, and resilience. TPA was widely tested by HSI in fish (Ma et al. 2017c), prawn (Dai et al. 2014), chicken (Xiong et al. 2015a), blueberry (Hu et al. 2015), melon (Sun et al. 2017a), wheat (Mahesh et al. 2015), pistachio kernel (Mohammadi-Moghaddam et al. 2018), and cheese (Vásquez et al. 2018). When comparing the best models, it should be pointed out that assessing the hardness of muscle foods and cheeses is more appropriate than doing so for fruits and cereals. In aquatic products, prediction in fish outperformed that in shrimp in TPA tests; in recently published papers, the performance of predicting gumminess was not acceptable in all aspects. However, tenderness, always a consumer concern in muscle foods, was commonly characterized by the WBSF or SSF assessment. The tenderness of beef (Naganathan et al. 2015, 2016; Nubiato et al. 2018; Qiao et al. 2015), pork (Tao & Peng 2014), chicken (Jiang et al. 2018), sea fish (He et al. 2014b), and river fish (Ma et al. 2017c) was evaluated by HSI. The results illustrated that the characteristic bands of predicted tenderness are concentrated in the ranges of 555–619 nm and 725–782 nm in the VIS–NIR region.

Others. In addition to the above, HSI can also contribute to the detection of other chemical or physical characteristics of foods. The anthocyanins are a group of vital phenolic components of red wine grapes that contribute significantly to the color of wine. Anthocyanin contents were predicted by HSI using the nonlinear predictive models of SVR (Chen et al. 2015) and ANN (Fernandes et al. 2015), with $R^2_p = 0.941$ and 0.95 in the spectral regions of 900–1,700 nm and 380–1,028 nm, respectively.

pH value is a key factor related to the quality and safety of food. The pH values of salt pork were investigated by spectral analysis only (Liu et al. 2014a) and by spectral analysis combined with image texture information (Liu et al. 2014b) in the spectral region of 400–1,000 nm. The results showed that texture information was useful to improve the model performance. Without

texture information, the predictions of pH values of salmon (He et al. 2014c), chicken (Jia et al. 2017), and wine grape berries (Fernandes et al. 2015) were inferior.

The color of food was studied in meat and meat products using HSI. Red meat, including fresh beef, lamb, and pork samples, was evaluated to predict color values, including L* (lightness), a* (red–green or redness), and b* (yellow–blue or yellowness), using the optimal wavelengths of 450, 460, 600, 620, 820, and 980 nm with a performance of $R^2_p > 0.82$ (Kamruzzaman et al. 2016). Similar results of $R^2_p > 0.816$ were obtained in predicting beef color (Liu et al. 2018b). It is also feasible to study the color value of frozen–thawed (Xie et al. 2015) and pickled pork meat (Liu et al. 2014a). Additionally, the drip losses of frozen-thawed pork (Xie et al. 2015) and cold-stored salmon (He et al. 2014c) were predicted. The gross energy density of salmon and the sterilization nonuniformity of microwaves were investigated by using HSI. Xu et al. (2016) developed an alternative technique to determine the gross energy density of salmon by using an NIR HSI ranging from 900 nm to 1,700 nm with an R_p of 0.909. The nonuniformity in microwave sterilization was screened by using HSI at wavelengths of 40 nm to 1,050 nm

Finally, the ripeness of fruit is one of the important factors that consumers consider when purchasing fruits. The ripeness of nectarine (Munera et al. 2017), persimmon (Wei et al. 2014), and strawberry (zhang et al. 2016) could be successfully predicted or classified by HSI.

Monitoring of Food Processes

During food processing, the main application of monitoring is to evaluate how the chemical or physical properties of food change during the process. HSI technology has great potential for online monitoring of changes in food quality and safety during food processing compared with other traditional food analysis methods. A recent review provides detailed information on quality and safety evaluation during various processes by HSI (Liu et al. 2017).

Thermal processing. Thermal processing is most commonly used for extending food shelf life and cooking. The thermal treatments of kamaboko (ElMasry & Nakauchi 2015), a kind of Japanese seafood, were monitored by HSI from 950 nm to 2,400 nm. The samples were heated in a small convection oven at different temperatures to obtain various cooked samples. The core temperature (T_C) and thermal history (TH) (calculated via the increase in temperature needed for a tenfold increase in the heating rate, the sample core temperature, and the period of reaching the set temperature) of samples were predicted. The results were acceptable, with an $R^2_p = 0.86$ for TC, and $R^2_p = 0.83$ for TH (ElMasry & Nakauchi 2015). The TVB-N content change of cured pork meat heated in an industrial drying room was also evaluated. Samples at different heating steps were taken out during drying for 48 h. A result of $R^2_p = 0.861$ was obtained by applying the MLR model based on optimal wavelengths (Yang et al. 2017b). Additionally, changes in the moisture content, color, and percentage of three myoglobins of beef samples were tested by HSI under microwave heating for 75 s (Liu et al. 2018b).

Freezing and chilling. Freezing and chilling are often used in the food industry, during which a series of chemical and physical changes occur. Four different initial freezing conditions were used to freeze pork samples, which were then stored in a freezer for 3 days at −20°C (Xie et al. 2015, 2016). HSI from 900 nm to 2,500 nm was shown to be able to predict L*, b*, a*, cooking loss, and drip loss of the frozen samples (Xie et al. 2015) as well as freezing parameters (Xie et al. 2016) without thawing the samples. Furthermore, short-time freezing and thawing alternation was applied to simulate possible temperature fluctuations during transportation; under these conditions, pork (Ma et al. 2015; Pu et al. 2014, 2015) and shrimp (Qu et al. 2015) were evaluated to identify the

effect of temperature fluctuations on samples. It was found that adding image texture information could improve the performance of classification models.

Dehydration. Dehydration is a conventional food preservation method and widely used for drying foods. Tea leaves were studied by investigating the color components (i.e., L*, a*, and b*) change during different drying periods using VIS–NIR HSI (Xie et al. 2014). In addition, microwave–vacuum drying is a new type of drying method that has been applied in mango drying. HSI was carried out to monitor the moisture distribution of mango during the drying period, and the results showed that the moisture content of the middle of the mango was lower than that of the parts on the periphery during the drying process (Pu & Sun 2015, 2017), as well as round-shaped mango slices achieved better drying results (Pu & Sun 2016). Furthermore, freeze-drying is a dehydration method that can protect food with minimal transformations in chemical composition, texture, flavor, and rehydration ability. Changes in moisture content (Qu et al. 2017), textural features (Ma et al. 2017c), and dehydration and rehydration (Ma et al. 2017a) of fish fillets were monitored by means of HSI during freeze-drying, and the results showed that the median spectra of the hyperspectral image had great potential to evaluate the textural features of freeze-dried fish fillets.

Food Safety Evaluation

Foodborne risks present a critical issue to public health. Therefore, it is important to evaluate food safety using reliable, effective, and exercisable methods. On the basis of the results of various studies, it is feasible to assess food safety by means of HSI.

Freshness evaluation. Food freshness is an important indicator for evaluating food safety, and the methods available are diverse. Generally, chemical component and physical changes and microbiological reproduction are the main parameters when monitoring the freshness of foods. Along with applications of HSI to investigate properties related to food freshness, including moisture, TVB-N, and TBA contents as discussed above, microbiological monitoring with HSI forms an important part of HSI applications in food safety evaluation.

The total viable count (TVC) can indicate the reproduction of microorganisms in food and whether the food is fresh or not. TVC in beef is determined by HSI according to the critical value of 106 CFU/g, with the algorithm combining wavelet transform and N-way partial least squares (N-PLS), and the best predictive model for TVC was established with $R^2_p = 0.934$ (Yang et al. 2018). In addition, HSI has also been used to evaluate the TVC of fish (Cheng & Sun 2015a), lamb (Duan et al. 2017), pork (Tao & Peng 2015, Zheng et al. 2017), chicken (Ye et al. 2016), and dried sausages (Siripatrawan 2018) and all the predictive models were built based on the spectral region from 400 nm to 1,000 nm. Furthermore, *Escherichia coli* content in fish was studied by selecting optimal wavelengths (424, 451, 545, 567, 585, and 610 nm) using the MLR model ($R^2_p = 0.870$) (Cheng & Sun 2015b). Furthermore, it is feasible for HSI to predict the lactic acid bacteria contents of salmon (He et al. 2014a) and *Acidovorax citrulli* contents of watermelon seeds (Lee et al. 2017).

Defect detection. The applications of HSI in defect detection normally focus on fruit and vegetables. External defects have negative effects on market value and consumer purchasing behavior, whereas internal defects are related to shelf life. In particular, it is difficult to identify internal defects by the human eye or RGB image-based computer vision techniques. Commonly, there are two typical strategies for determining the defects of food using HSI: the chemometric model

analysis, which is based on spectral information of optimal wavelengths, and image identification, which is based on optimal wavelengths and imaging transformation algorithms. A few applications are available using the first strategy to detect bruises and defects of apple (Zhu et al. 2016), jujube (Wu et al. 2016a), and white maize (Sendin et al. 2018).

Most of the applications are achieved by image identification. First, the images at optimal wavelengths extracted from the region of 1,100–1,400 nm usually correspond to the bruises of fruits, including apple (Keresztes et al. 2016, 2017) and blueberry (Jiang et al. 2016). Second, band-ratio-transformed images are employed to detect internal attributes, such as internal defects in pickling cucumbers (Cen et al. 2014) and internal bruises in blueberries (Fan et al. 2017). PCA-transformed images are widely used in defect detection. Bruises (Che et al. 2018, Huang et al. 2015) and defects (Zhang et al. 2018) of apples were easily identified in the PC images in the 400–1,000 nm region. It is also feasible to detect bruises in banana (Wang et al. 2015) and early bruising (Li et al. 2018) and skin defects (Li et al. 2016b) in peaches using PC images. Additionally, minimum noise fraction transformed images were used to determine the defects in peaches and loquats (Yu et al. 2014) and bruises in strawberries (Liu et al. 2018a). Finally, black spots in potatoes were successfully identified by HSI (López-Maestresalas et al. 2016). The model accuracies of all the above applications were as high as 0.9, showing that HSI is a reliable method to detect the defects in fruit and vegetables.

CONCLUSIONS AND FUTURE TRENDS

HSI technology has become a hot spot for food quality and safety detection. It combines two traditional techniques: spectroscopy and computer vision. Hyperspectral images contain rich physicochemical information about food samples. The combination of cross-cutting technologies can complement each other and produce more powerful technologies.

The 3D data cube of the hyperspectral image contains abundant physical and chemical information about food. Multiple mathematical algorithms can be applied to assist researchers in understanding HSI, and many applications have demonstrated its feasibility to evaluate numerous properties of various foods.

Future developments in HSI technology may combine the technology with other nondestructive testing methods, including the electronic nose and ultrasound imaging technology. In addition, the spectral electromagnetic wave range in HSI technology can be expanded, and the confocal principle can be used to obtain more internal information about foods. It is also necessary to make efforts to improve the algorithms. Finally, by combining big data and cloud-computing technologies, the hyperspectral data from different research teams could be shared so that the technology can be advanced further.

DISCLOSURE STATEMENT

The authors are not aware of any affiliations, memberships, funding, or financial holdings that might be perceived as affecting the objectivity of this review.

ACKNOWLEDGMENTS

The authors are grateful to the National Key R&D Program of China (2017YFD0400404) for its support. This research was also supported by the Collaborative Innovation Major Special Projects of Guangzhou City (201604020007), the Guangdong Provincial Science and Technology Plan

Projects (2015A020209016, 2016A040403040), the Fundamental Research Funds for the Central Universities (2017MS067, 2017MS075), the International and Hong Kong–Macau–Taiwan Collaborative Innovation Platform of Guangdong Province on Intelligent Food Quality Control and Process Technology & Equipment (2015KGJHZ001), the Guangdong Provincial R&D Centre for the Modern Agricultural Industry on Non-Destructive Detection and Intensive Processing of Agricultural Products, the Common Technical Innovation Team of Guangdong Province on Preservation and Logistics of Agricultural Products (2016LM2154), and the Innovation Centre of Guangdong Province for Modern Agricultural Science and Technology on Intelligent Sensing and Precision Control of Agricultural Product Qualities.

LITERATURE CITED

Amjad W, Crichton SO, Munir A, Hensel O, Sturm B. 2018. Hyperspectral imaging for the determination of potato slice moisture content and chromaticity during the convective hot air drying process. *Biosyst. Eng.* 166:170–83

Araújo MCU, Saldanha TCB, Galvão RKH, Yoneyama T, Chame HC, Visani V. 2001. The successive projections algorithm for variable selection in spectroscopic multicomponent analysis. *Chemom. Intell. Lab. Syst.* 57:65–73

Barnes RJ, Dhanoa MS, Lister SJ. 1989. Standard normal variate transformation and de-trending of near-infrared diffuse reflectance spectra. *Appl. Spectrosc.* 43:772–77

Caporaso N, Whitworth MB, Fisk ID. 2018a. Protein content prediction in single wheat kernels using hyperspectral imaging. *Food Chem.* 240:32–42

Caporaso N, Whitworth MB, Grebby S, Fisk ID. 2018b. Rapid prediction of single green coffee bean moisture and lipid content by hyperspectral imaging. *J. Food Eng.* 227:18–29

Cen H, Lu R, Ariana DP, Mendoza F. 2014. Hyperspectral imaging-based classification and wavebands selection for internal defect detection of pickling cucumbers. *Food Bioprocess Technol.* 7:1689–700

Centner V, Massart D-L, de Noord OE, de Jong S, Vandeginste BM, Sterna C. 1996. Elimination of Uninformative Variables for Multivariate Calibration. *Anal. Chem.* 68:3851–58

Che W, Sun L, Zhang Q, Tan W, Ye D, et al. 2018. Pixel based bruise region extraction of apple using Vis-NIR hyperspectral imaging. *Comput. Electron. Agric.* 146:12–21

Chen S, Zhang F, Ning J, Liu X, Zhang Z, Yang S. 2015. Predicting the anthocyanin content of wine grapes by NIR hyperspectral imaging. *Food Chem.* 172:788–93

Chen X, Lei X. 2009. Application of a hybrid variable selection method for determination of carbohydrate content in soy milk powder using visible and near infrared spectroscopy. *J. Agric. Food Chem.* 57:334–40

Cheng J-H, Sun D-W. 2015a. Rapid and non-invasive detection of fish microbial spoilage by visible and near infrared hyperspectral imaging and multivariate analysis. *LWT Food Sci. Technol.* 62:1060–68

Cheng J-H, Sun D-W. 2015b. Rapid quantification analysis and visualization of *Escherichia coli* loads in grass carp fish flesh by hyperspectral imaging method. *Food Bioprocess Technol.* 8:951–59

Cheng J-H, Sun D-W, Liu G, Chen YN. 2019. Developing a multispectral model for detection of docosahexaenoic acid (DHA) and eicosapentaenoic acid (EPA) changes in fish fillet using physarum network and genetic algorithm (PN-GA) method. *Food Chem.* 270:181–88

Cheng J-H, Sun D-W, Pu H-B, Wang Q-J, Chen Y-N. 2015. Suitability of hyperspectral imaging for rapid evaluation of thiobarbituric acid (TBA) value in grass carp (*Ctenopharyngodon idella*) fillet. *Food Chem.* 171:258–65

Cheng J-H, Sun D-W, Wei Q. 2017. Enhancing visible and near-infrared hyperspectral imaging prediction of TVB-N Level for fish fillet freshness evaluation by filtering optimal variables. *Food Anal. Methods* 10:1888–98

Cheng J-H, Sun D-W, Zeng X-A, Pu H-B. 2014. Non-destructive and rapid determination of TVB-N content for freshness evaluation of grass carp (*Ctenopharyngodon idella*) by hyperspectral imaging. *Innov. Food Sci. Emerg. Technol.* 21:179–87

Cheng W, Sun D-W, Pu H, Wei Q. 2017. Chemical spoilage extent traceability of two kinds of processed pork meats using one multispectral system developed by hyperspectral imaging combined with effective variable selection methods. *Food Chem*. 221:1989–96

Cheng W, Sun D-W, Pu H, Wei Q. 2018a. Characterization of myofibrils cold structural deformation degrees of frozen pork using hyperspectral imaging coupled with spectral angle mapping algorithm. *Food Chem*. 239:1001–8

Cheng W, Sun D-W, Pu H, Wei Q. 2018b. Heterospectral two-dimensional correlation analysis with near-infrared hyperspectral imaging for monitoring oxidative damage of pork myofibrils during frozen storage. *Food Chem*. 248:119–27

Cluff K, Konda Naganathan G, Subbiah J, Lu R, Calkins CR, Samal A. 2008. Optical scattering in beef steak to predict tenderness using hyperspectral imaging in the VIS-NIR region. *Sens. Instrum. Food Qual. Saf.* 2:189–96

Cortés V, Blasco J, Aleixos N, Cubero S, Talens P. 2017. Visible and near-infrared diffuse reflectance spectroscopy for fast qualitative and quantitative assessment of nectarine quality. *Food Bioprocess Technol*. 10:1755–66

Craigie C, Johnson P, Shorten P, Charteris A, Maclennan G, et al. 2017. Application of hyperspectral imaging to predict the pH, intramuscular fatty acid content and composition of lamb M. longissimus lumborum at 24 h post mortem. *Meat Sci*. 132:19–28

Crichton S, Shrestha L, Hurlbert A, Sturm B. 2017. Use of hyperspectral imaging for the prediction of moisture content and chromaticity of raw and pretreated apple slices during convection drying. *Dry. Technol.* 36:804–16

Dai Q, Cheng J-H, Sun D-W, Pu H, Zeng X-A, Xiong Z. 2015. Potential of visible/near-infrared hyperspectral imaging for rapid detection of freshness in unfrozen and frozen prawns. *J. Food Eng.* 149:97–104

Dai Q, Cheng J-H, Sun D-W, Zeng X-A. 2014. Potential of hyperspectral imaging for non-invasive determination of mechanical properties of prawn (*Metapenaeus ensis*). *J. Food Eng.* 136:64–72

Deng S, Xu Y, Li X, He Y. 2015. Moisture content prediction in tealeaf with near infrared hyperspectral imaging. *Comput. Electron. Agric.* 118:38–46

Duan HW, Zhu RG, Yao XD, Lewis E. 2017. Sensitive variables extraction, non-destructive detection and visualization of total viable count (TVC) and pH in vacuum packaged lamb using hyperspectral imaging. *Anal. Methods* 9:3172–83

ElMasry G, Nakauchi S. 2015. Noninvasive sensing of thermal treatments of Japanese seafood products using imaging spectroscopy. *Int. J. Food Sci. Technol.* 50:1960–71

Fan S, Huang W, Guo Z, Zhang B, Zhao C. 2015. Prediction of soluble solids content and firmness of pears using hyperspectral reflectance imaging. *Food Anal. Methods* 8:1936–46

Fan S, Li C, Huang W, Chen L. 2017. Detection of blueberry internal bruising over time using NIR hyperspectral reflectance imaging with optimum wavelengths. *Postharvest Biol. Technol.* 134:55–66

Fan S, Zhang B, Li J, Huang W, Wang C. 2016a. Effect of spectrum measurement position variation on the robustness of NIR spectroscopy models for soluble solids content of apple. *Biosyst. Eng.* 143:9–19

Fan S, Zhang B, Li J, Liu C, Huang W, Tian X. 2016b. Prediction of soluble solids content of apple using the combination of spectra and textural features of hyperspectral reflectance imaging data. *Postharvest Biol. Technol.* 121:51–61

Fernandes AM, Franco C, Mendes-Ferreira A, Mendes-Faia A, da Costa PL, Melo-Pinto P. 2015. Brix, pH and anthocyanin content determination in whole Port wine grape berries by hyperspectral imaging and neural networks. *Comput. Electron. Agric.* 115:88–96

Garrido-Novell C, Garrido-Varo A, Pérez-Marín D, Guerrero-Ginel J, Kim M. 2015. Quantification and spatial characterization of moisture and NaCl content of Iberian dry-cured ham slices using NIR hyperspectral imaging. *J. Food Eng.* 153:117–23

Garrido-Novell C, Garrido-Varo A, Pérez-Marín D, Guerrero JE. 2018. Using spectral and textural data extracted from hyperspectral near infrared spectroscopy imaging to discriminate between processed pork, poultry and fish proteins. *Chemom. Intell. Lab. Syst.* 172:90–99

Guo T, Huang M, Zhu Q, Guo Y, Qin J. 2018. Hyperspectral image-based multi-feature integration for TVB-N measurement in pork. *J. Food Eng.* 218:61–68

Guo W, Zhao F, Dong J. 2016. Nondestructive measurement of soluble solids content of kiwifruits using near-infrared hyperspectral imaging. *Food Anal. Methods* 9:38–47

He H-J, Sun D-W, Wu D. 2014a. Rapid and real-time prediction of lactic acid bacteria (LAB) in farmed salmon flesh using near-infrared (NIR) hyperspectral imaging combined with chemometric analysis. *Food Res. Int.* 62:476–83

He H-J, Wu D, Sun D-W. 2014b. Potential of hyperspectral imaging combined with chemometric analysis for assessing and visualising tenderness distribution in raw farmed salmon fillets. *J. Food Eng.* 126:156–64

He H-J, Wu D, Sun D-W. 2014c. Rapid and non-destructive determination of drip loss and pH distribution in farmed Atlantic salmon (*Salmo salar*) fillets using visible and near-infrared (Vis–NIR) hyperspectral imaging. *Food Chem.* 156:394–401

Hu M-H, Dong Q-L, Liu B-L, Opara UL, Chen L. 2015. Estimating blueberry mechanical properties based on random frog selected hyperspectral data. *Postharvest Biol. Technol.* 106:1–10

Hu W, Sun D-W, Blasco J. 2017. Rapid monitoring 1-MCP-induced modulation of sugars accumulation in ripening 'Hayward' kiwifruit by Vis/NIR hyperspectral imaging. *Postharvest Biol. Technol.* 125:168–80

Huang M, Wang Q, Zhang M, Zhu Q. 2014. Prediction of color and moisture content for vegetable soybean during drying using hyperspectral imaging technology. *J. Food Eng.* 128:24–30

Huang W, Li J, Wang Q, Chen L. 2015. Development of a multispectral imaging system for online detection of bruises on apples. *J. Food Eng.* 146:62–71

Isaksson T, Næs T. 1988. The effect of multiplicative scatter correction (MSC) and linearity improvement in NIR spectroscopy. *Appl. Spectrosc.* 42:1273–84

Izenman AJ. 2008. Linear discriminant analysis. In *Modern Multivariate Statistical Techniques: Regression, Classification, and Manifold Learning*, pp. 237–80. New York: Springer

Jia B, Yoon S-C, Zhuang H, Wang W, Li C. 2017. Prediction of pH of fresh chicken breast fillets by VNIR hyperspectral imaging. *J. Food Eng.* 208:57–65

Jiang H, Yoon S-C, Zhuang H, Wang W, Lawrence KC, Yang Y. 2018. Tenderness classification of fresh broiler breast fillets using visible and near-infrared hyperspectral imaging. *Meat Sci.* 139:82–90

Jiang Y, Li CY, Takeda F. 2016. Nondestructive detection and quantification of blueberry bruising using near-infrared (NIR) hyperspectral reflectance imaging. *Sci. Rep.* 6:35679

Jin H, Li L, Cheng J. 2015. Rapid and non-destructive determination of moisture content of peanut kernels using hyperspectral imaging technique. *Food Anal. Methods* 8:2524–32

Kamruzzaman M, Makino Y, Oshita S. 2016. Online monitoring of red meat color using hyperspectral imaging. *Meat Sci.* 116:110–17

Keresztes JC, Diels E, Goodarzi M, Nguyen-Do-Trong N, Goos P, et al. 2017. Glare based apple sorting and iterative algorithm for bruise region detection using shortwave infrared hyperspectral imaging. *Postharvest Biol. Technol.* 130:103–15

Keresztes JC, Goodarzi M, Saeys W. 2016. Real-time pixel based early apple bruise detection using short wave infrared hyperspectral imaging in combination with calibration and glare correction techniques. *Food Control* 66:215–26

Khulal U, Zhao J, Hu W, Chen Q. 2016. Nondestructive quantifying total volatile basic nitrogen (TVB-N) content in chicken using hyperspectral imaging (HSI) technique combined with different data dimension reduction algorithms. *Food Chem.* 197:1191–99

Khulal U, Zhao J, Hu W, Chen Q. 2017. Intelligent evaluation of total volatile basic nitrogen (TVB-N) content in chicken meat by an improved multiple level data fusion model. *Sensors Actuators B* 238:337–45

Kjær A, Nielsen G, Stærke S, Clausen MR, Edelenbos M, Jørgensen B. 2016. Prediction of starch, soluble sugars and amino acids in potatoes (*Solanum tuberosum* L.) using hyperspectral imaging, dielectric and LF-NMR methodologies. *Potato Res.* 59:357–74

Leardi R, Boggia R, Terrile M. 1992. Genetic algorithms as a strategy for feature selection. *J. Chemom.* 6:267–81

Lee H, Kim MS, Lee W-H, Cho B-K. 2018. Determination of the total volatile basic nitrogen (TVB-N) content in pork meat using hyperspectral fluorescence imaging. *Sensors Actuators B* 259:532–39

Lee H, Kim MS, Song YR, Oh CS, Lim HS, et al. 2017. Non-destructive evaluation of bacteria-infected watermelon seeds using visible/near-infrared hyperspectral imaging. *J. Sci. Food Agric.* 97:1084–92

Li B, Hou B, Zhang D, Zhou Y, Zhao M, et al. 2016a. Pears characteristics (soluble solids content and firmness prediction, varieties) testing methods based on visible-near infrared hyperspectral imaging. *Int. J. Light Electron Opt.* 127:2624–30

Li H, Chen Q, Zhao J, Wu M. 2015. Nondestructive detection of total volatile basic nitrogen (TVB-N) content in pork meat by integrating hyperspectral imaging and colorimetric sensor combined with a nonlinear data fusion. *LWT Food Sci. Technol.* 63:268–74

Li J, Chen L. 2017. Comparative analysis of models for robust and accurate evaluation of soluble solids content in 'Pinggu' peaches by hyperspectral imaging. *Comput. Electron. Agric.* 142:524–35

Li J, Chen L, Huang W. 2018. Detection of early bruises on peaches (*Amygdalus persica* L.) using hyperspectral imaging coupled with improved watershed segmentation algorithm. *Postharvest Biol. Technol.* 135:104–13

Li J, Chen L, Huang W, Wang Q, Zhang B, et al. 2016b. Multispectral detection of skin defects of bi-colored peaches based on vis–NIR hyperspectral imaging. *Postharvest Biol. Technol.* 112:121–33

Li J, Tian X, Huang W, Zhang B, Fan S. 2016c. Application of long-wave near infrared hyperspectral imaging for measurement of soluble solid content (SSC) in pear. *Food Anal. Methods* 9:3087–98

Liu D, Ma J, Sun D-W, Pu H, Gao W, et al. 2014a. Prediction of color and pH of salted porcine meats using visible and near-infrared hyperspectral imaging. *Food Bioprocess Technol.* 7:3100–8

Liu D, Pu H, Sun D-W, Wang L, Zeng X-A. 2014b. Combination of spectra and texture data of hyperspectral imaging for prediction of pH in salted meat. *Food Chem.* 160:330–37

Liu D, Sun D-W, Qu J, Zeng X-A, Pu H, Ma J. 2014c. Feasibility of using hyperspectral imaging to predict moisture content of porcine meat during salting process. *Food Chem.* 152:197–204

Liu D, Sun D-W, Zeng X-A. 2014d. Recent advances in wavelength selection techniques for hyperspectral image processing in the food industry. *Food Bioprocess Technol.* 7:307–23

Liu Q, Sun K, Peng J, Xing M, Pan L, Tu K. 2018a. Identification of bruise and fungi contamination in strawberries using hyperspectral imaging technology and multivariate analysis. *Food Anal. Methods* 11:1518–27

Liu Y, Pu H, Sun D-W. 2017. Hyperspectral imaging technique for evaluating food quality and safety during various processes: a review of recent applications. *Trends Food Sci. Technol.* 69:25–35

Liu Y, Sun D-W, Cheng J-H, Han Z. 2018b. Hyperspectral imaging sensing of changes in moisture content and color of beef during microwave heating process. *Food Anal. Methods* 11:2472–84

Lohumi S, Lee S, Lee H, Kim MS, Lee W-H, Cho B-K. 2016. Application of hyperspectral imaging for characterization of intramuscular fat distribution in beef. *Infrared Phys. Technol.* 74:1–10

López-Maestresalas A, Keresztes JC, Goodarzi M, Arazuri S, Jarén C, Saeys W. 2016. Non-destructive detection of blackspot in potatoes by Vis-NIR and SWIR hyperspectral imaging. *Food Control* 70:229–41

Ma J, Pu H, Sun D-W. 2018. Predicting intramuscular fat content variations in boiled pork muscles by hyperspectral imaging using a novel spectral pre-processing technique. *LWT Food Sci. Technol.* 94:119–28

Ma J, Pu H, Sun D-W, Gao W, Qu J-H, Ma K-Y. 2015. Application of Vis–NIR hyperspectral imaging in classification between fresh and frozen-thawed pork longissimus dorsi muscles. *Int. J. Refrig.* 50:10–18

Ma J, Qu J-H, Sun D-W. 2017a. Developing hyperspectral prediction model for investigating dehydrating and rehydrating mass changes of vacuum freeze dried grass carp fillets. *Food Bioprod. Process.* 104:66–76

Ma J, Sun D-W, Pu H. 2016. Spectral absorption index in hyperspectral image analysis for predicting moisture contents in pork longissimus dorsi muscles. *Food Chem.* 197:848–54

Ma J, Sun D-W, Pu H. 2017b. Model improvement for predicting moisture content (MC) in pork longissimus dorsi muscles under diverse processing conditions by hyperspectral imaging. *J. Food Eng.* 196:65–72

Ma J, Sun D-W, Pu H, Wei Q, Wang X. 2019. Protein content evaluation of processed pork meats based on a novel single shot (snapshot) hyperspectral imaging sensor. *J. Food Eng.* 240:207–13

Ma J, Sun D-W, Qu J-H, Pu H. 2017c. Prediction of textural changes in grass carp fillets as affected by vacuum freeze drying using hyperspectral imaging based on integrated group wavelengths. *LWT Food Sci. Technol.* 82:377–85

Ma T, Li X, Inagaki T, Yang H, Tsuchikawa S. 2017d. Noncontact evaluation of soluble solids content in apples by near-infrared hyperspectral imaging. *J. Food Eng.* 224:53–61

Mahesh S, Jayas D, Paliwal J, White N. 2015. Comparison of partial least squares regression (PLSR) and principal components regression (PCR) methods for protein and hardness predictions using the near-infrared (NIR) hyperspectral images of bulk samples of Canadian wheat. *Food Bioprocess Technol.* 8:31–40

Mohammadi-Moghaddam T, Razavi SM, Taghizadeh M, Pradhan B, Sazgarnia A, Shaker-Ardekani A. 2018. Hyperspectral imaging as an effective tool for prediction the moisture content and textural characteristics of roasted pistachio kernels. *J. Food Meas. Char.* 12:1493–502

Munera S, Amigo JM, Blasco J, Cubero S, Talens P, Aleixos N. 2017. Ripeness monitoring of two cultivars of nectarine using VIS-NIR hyperspectral reflectance imaging. *J. Food Eng.* 214:29–39

Naganathan GK, Cluff K, Samal A, Calkins CR, Jones DD, et al. 2015. Hyperspectral imaging of ribeye muscle on hanging beef carcasses for tenderness assessment. *Comput. Electron. Agric.* 116:55–64

Naganathan GK, Cluff K, Samal A, Calkins CR, Jones DD, et al. 2016. Three dimensional chemometric analyses of hyperspectral images for beef tenderness forecasting. *J. Food Eng.* 169:309–20

Nicolaï BM, Beullens K, Bobelyn E, Peirs A, Saeys W, et al. 2007. Nondestructive measurement of fruit and vegetable quality by means of NIR spectroscopy: a review. *Postharvest Biol. Technol.* 46:99–118

Norgaard L, Saudland A, Wagner J, Nielsen JP, Munck L, Engelsen SB. 2000. Interval partial least-squares regression (iPLS): a comparative chemometric study with an example from near-infrared spectroscopy. *Appl. Spectrosc.* 54:413–19

Nubiato KEZ, Mazon MR, Antonelo DS, Calkins CR, Naganathan GK, et al. 2018. A bench-top hyperspectral imaging system to classify beef from Nellore cattle based on tenderness. *Infrared Phys. Technol.* 89:247–54

Park B, Yoon S-C, Windham WR, Lawrence KC, Kim MS, Chao K. 2011. Line-scan hyperspectral imaging for real-time in-line poultry fecal detection. *Sens. Instrum. Food Qual. Safety* 5:25–32

Pu H, Liu D, Wang L, Sun D-W. 2016. Soluble solids content and pH prediction and maturity discrimination of lychee fruits using visible and near infrared hyperspectral imaging. *Food Anal. Methods* 9:235–44

Pu H, Sun D-W, Ma J, Cheng J-H. 2015. Classification of fresh and frozen-thawed pork muscles using visible and near infrared hyperspectral imaging and textural analysis. *Meat Sci.* 99:81–88

Pu H, Sun D-W, Ma J, Liu D, Cheng J-H. 2014. Using wavelet textural features of visible and near infrared hyperspectral image to differentiate between fresh and frozen–thawed pork. *Food Bioprocess Technol.* 7:3088–99

Pu Y-Y, Sun D-W. 2015. Vis–NIR hyperspectral imaging in visualizing moisture distribution of mango slices during microwave-vacuum drying. *Food Chem.* 188:271–78

Pu Y-Y, Sun D-W. 2016. Prediction of moisture content uniformity of microwave-vacuum dried mangoes as affected by different shapes using NIR hyperspectral imaging. *Innov. Food Sci. Emerg. Technol.* 33:348–56

Pu Y-Y, Sun D-W. 2017. Combined hot-air and microwave-vacuum drying for improving drying uniformity of mango slices based on hyperspectral imaging visualisation of moisture content distribution. *Biosyst. Eng.* 156:108–19

Pu Y-Y, Sun D-W, Riccioli C, Buccheri M, Grassi M, et al. 2018. Calibration transfer from micro NIR spectrometer to hyperspectral imaging: a case study on predicting soluble solids content of bananito fruit (*Musa acuminata*). *Food Anal. Methods* 11:1021–33

Qiao L, Tang X, Dong J. 2017. A feasibility quantification study of total volatile basic nitrogen (TVB-N) content in duck meat for freshness evaluation. *Food Chem.* 237:1179–85

Qiao T, Ren J, Craigie C, Zabalza J, Maltin C, Marshall S. 2015. Singular spectrum analysis for improving hyperspectral imaging based beef eating quality evaluation. *Comput. Electron. Agric.* 115:21–25

Qu J-H, Cheng J-H, Sun D-W, Pu H, Wang Q-J, Ma J. 2015. Discrimination of shelled shrimp (*Metapenaeus ensis*) among fresh, frozen-thawed and cold-stored by hyperspectral imaging technique. *LWT Food Sci. Technol.* 62:202–9

Qu J-H, Sun D-W, Cheng J-H, Pu H. 2017. Mapping moisture contents in grass carp (*Ctenopharyngodon idella*) slices under different freeze drying periods by Vis-NIR hyperspectral imaging. *LWT Food Sci. Technol.* 75:529–36

Rady A, Guyer D, Lu R. 2015. Evaluation of sugar content of potatoes using hyperspectral imaging. *Food Bioprocess Technol.* 8:995–1010

Rahman A, Kandpal LM, Lohumi S, Kim MS, Lee H, et al. 2017. Nondestructive estimation of moisture content, PH and soluble solid contents in intact tomatoes using hyperspectral imaging. *Appl. Sci.* 7:109

Rossi F, Lendasse A, François D, Wertz V, Verleysen M. 2006. Mutual information for the selection of relevant variables in spectrometric nonlinear modelling. *Chemom. Intell. Lab. Syst.* 80:215–26

Sendin K, Manley M, Williams PJ. 2018. Classification of white maize defects with multispectral imaging. *Food Chem*. 243:311–18

Shi J, Hu X, Zou X, Zhao J, Zhang W, et al. 2017. A rapid and nondestructive method to determine the distribution map of protein, carbohydrate and sialic acid on edible bird's nest by hyper-spectral imaging and chemometrics. *Food Chem*. 229:235–41

Siripatrawan U. 2018. Hyperspectral imaging for rapid evaluation and visualization of quality deterioration index of vacuum packaged dry-cured sausages. *Sensors Actuators B* 254:1025–32

Su W-H, Sun D-W. 2017. Evaluation of spectral imaging for inspection of adulterants in terms of common wheat flour, cassava flour and corn flour in organic Avatar wheat (*Triticum* spp.) flour. *J. Food Eng.* 200:59–69

Sun M, Zhang D, Liu L, Wang Z. 2017a. How to predict the sugariness and hardness of melons: a near-infrared hyperspectral imaging method. *Food Chem*. 218:413–21

Sun Y, Liu Y, Yu H, Xie A, Li X, et al. 2017b. Non-destructive prediction of moisture content and freezable water content of purple-fleshed sweet potato slices during drying process using hyperspectral imaging technique. *Food Anal. Methods* 10:1535–46

Tao F, Mba O, Liu L, Ngadi M. 2017. Rapid and non-destructive assessment of polyunsaturated fatty acids contents in salmon using near-infrared hyperspectral imaging. In *Hyperspectral Imaging Sensors: Innovative Applications and Sensor Standards*, ed. DP Bannon. Bellingham, WA: SPIE

Tao F, Peng Y. 2014. A method for nondestructive prediction of pork meat quality and safety attributes by hyperspectral imaging technique. *J. Food Eng.* 126:98–106

Tao F, Peng Y. 2015. A nondestructive method for prediction of total viable count in pork meat by hyperspectral scattering imaging. *Food Bioprocess Technol*. 8:17–30

Teerachaichayut S, Ho HT. 2017. Non-destructive prediction of total soluble solids, titratable acidity and maturity index of limes by near infrared hyperspectral imaging. *Postharvest Biol. Technol.* 133:20–25

Vapnik V. 2013. *The Nature of Statistical Learning Theory*. Berlin, Ger.: Springer Sci.

Vásquez N, Magán C, Oblitas J, Chuquizuta T, Avila-George H, Castro W. 2018. Comparison between artificial neural network and partial least squares regression models for hardness modeling during the ripening process of Swiss-type cheese using spectral profiles. *J. Food Eng.* 219:8–15

Velásquez L, Cruz-Tirado J, Siche R, Quevedo R. 2017. An application based on the decision tree to classify the marbling of beef by hyperspectral imaging. *Meat Sci*. 133:43–50

Vidal A, Talens P, Prats-Montalbán JM, Cubero S, Albert F, Blasco J. 2013. In-line estimation of the standard colour index of citrus fruits using a computer vision system developed for a mobile platform. *Food Bioprocess Technol*. 6:3412–19

Wang N-N, Yang Y-C, Sun D-W, Pu H, Zhu Z. 2015. Shelf-life prediction of 'Gros Michel' bananas with different browning levels using hyperspectral reflectance imaging. *Food Anal. Methods* 8:1173–84

Wei X, Liu F, Qiu Z, Shao Y, He Y. 2014. Ripeness classification of astringent persimmon using hyperspectral imaging technique. *Food Bioprocess Technol*. 7:1371–80

Wold S, Esbensen K, Geladi P. 1987. Principal component analysis. *Chemom. Intell. Lab. Syst.* 2:37–52

Wood J, Richardson R, Nute G, Fisher A, Campo M, et al. 2004. Effects of fatty acids on meat quality: a review. *Meat Sci*. 66:21–32

Wu D, Sun D-W. 2013. Advanced applications of hyperspectral imaging technology for food quality and safety analysis and assessment: a review—Part I: fundamentals. *Innov. Food Sci. Emerg. Technol.* 19:1–14

Wu L, He J, Liu G, Wang S, He X. 2016a. Detection of common defects on jujube using Vis-NIR and NIR hyperspectral imaging. *Postharvest Biol. Technol.* 112:134–42

Wu X, Song X, Qiu Z, He Y. 2016b. Mapping of TBARS distribution in frozen–thawed pork using NIR hyperspectral imaging. *Meat Sci*. 113:92–96

Xie A, Sun D-W, Xu Z, Zhu Z. 2015. Rapid detection of frozen pork quality without thawing by Vis–NIR hyperspectral imaging technique. *Talanta* 139:208–15

Xie A, Sun D-W, Zhu Z, Pu H. 2016. Nondestructive measurements of freezing parameters of frozen porcine meat by NIR hyperspectral imaging. *Food Bioprocess Technol*. 9:1444–54

Xie CQ, Li XL, Shao YN, He Y. 2014. Color measurement of tea leaves at different drying periods using hyperspectral imaging technique. *PLOS ONE* 9(12):e113422

Xiong Z, Sun D-W, Dai Q, Han Z, Zeng X-A, Wang L. 2015a. Application of visible hyperspectral imaging for prediction of springiness of fresh chicken meat. *Food Anal. Methods* 8:380–91

Xiong Z, Sun D-W, Pu H, Xie A, Han Z, Luo M. 2015b. Non-destructive prediction of thiobarbituric acid reactive substances (TBARS) value for freshness evaluation of chicken meat using hyperspectral imaging. *Food Chem*. 179:175–81

Xiong Z, Sun D-W, Xie A, Han Z, Wang L. 2015c. Potential of hyperspectral imaging for rapid prediction of hydroxyproline content in chicken meat. *Food Chem*. 175:417–22

Xu J-L, Riccioli C, Sun D-W. 2016. Development of an alternative technique for rapid and accurate determination of fish caloric density based on hyperspectral imaging. *J. Food Eng.* 190:185–94

Yan L, Xiong C, Qu H, Liu C, Chen W, Zheng L. 2017. Non-destructive determination and visualisation of insoluble and soluble dietary fibre contents in fresh-cut celeries during storage periods using hyperspectral imaging technique. *Food Chem*. 228:249–56

Yang D, He D, Lu A, Ren D, Wang J. 2017a. Combination of spectral and textural information of hyperspectral imaging for the prediction of the moisture content and storage time of cooked beef. *Infrared Phys. Technol.* 83:206–16

Yang D, Lu A, Ren D, Wang J. 2018. Detection of total viable count in spiced beef using hyperspectral imaging combined with wavelet transform and multiway partial least squares algorithm. *J. Food Saf.* 38:e12390

Yang Q, Sun D-W, Cheng W. 2017b. Development of simplified models for nondestructive hyperspectral imaging monitoring of TVB-N contents in cured meat during drying process. *J. Food Eng.* 192:53–60

Yang Y-C, Sun D-W, Wang N-N. 2015. Rapid detection of browning levels of lychee pericarp as affected by moisture contents using hyperspectral imaging. *Comput. Electron. Agric.* 113:203–12

Ye X, Iino K, Zhang S. 2016. Monitoring of bacterial contamination on chicken meat surface using a novel narrowband spectral index derived from hyperspectral imagery data. *Meat Sci*. 122:25–31

Yu H, Liu H, Wang N, Yang Y, Shi A, et al. 2016. Rapid and visual measurement of fat content in peanuts by using the hyperspectral imaging technique with chemometrics. *Anal. Methods* 8:7482–92

Yu K-Q, Zhao Y-R, Liu Z-Y, Li X-L, Liu F, He Y. 2014. Application of visible and near-infrared hyperspectral imaging for detection of defective features in loquat. *Food Bioprocess Technol*. 7:3077–87

Zhang B, Liu L, Gu B, Zhou J, Huang J, Tian G. 2018. From hyperspectral imaging to multispectral imaging: portability and stability of HIS-MIS algorithms for common defect detection. *Postharvest Biol. Technol.* 137:95–105

zhang C, Guo C, Liu F, Kong W, He Y, Lou B. 2016. Hyperspectral imaging analysis for ripeness evaluation of strawberry with support vector machine. *J. Food Eng.* 179:11–18

Zhao M, Esquerre C, Downey G, O'Donnell CP. 2017. Process analytical technologies for fat and moisture determination in ground beef: a comparison of guided microwave spectroscopy and near infrared hyperspectral imaging. *Food Control* 73:1082–94

Zheng X, Peng Y, Li Y, Chao K, Qin J. 2017. Nondestructive detection of total viable count of chilled pork in high oxygen storage condition based on hyperspectral technology. In *Proceedings of SPIE Commercial + Scientific Sensing and Imaging*, vol. 10217, ed. MS Kim, K Chao, BA Chin, B-K Cho. Bellingham, WA: SPIE

Zhu F, Zhang H, Shao Y, He Y, Ngadi M. 2014. Mapping of fat and moisture distribution in Atlantic salmon using near-infrared hyperspectral imaging. *Food Bioprocess Technol*. 7:1208–14

Zhu Q, Guan J, Huang M, Lu R, Mendoza F. 2016. Predicting bruise susceptibility of 'Golden Delicious' apples using hyperspectral scattering technique. *Postharvest Biol. Technol.* 114:86–94